GMR
The Original

HIGH-EFFICIENCY OPTIMIZATION OF LEAD-FREE SN-BASED PEROVSKITE SOLAR CELLS USING SCAPS-1D

Awais Maqsood[1], Farhan Ali[2], Muhammad Ilyas[3], Hasnain Kashif[1], Shakeel Ahmad[4], Muhammad Ali[4], Husnain Ali[3], Muhammad Ilyas[5]

[1]EE Deptt. SEN, University of Management and Technology, Lahore 54770, Pakistan; awais.maqsood@umt.edu.pk (A.M); Hasnain.kashif@umt.edu.pk (H.K)
[2]School of Computer and IT, Beaconhouse National University, P.O. Box 53700 Lahore, Pakistan farhan32748@gmail.com (F.A)
[3]Department of software engineering, Superior University, Lahore 54000 Pakistan; muhammad.ilyas@superior.edu.pk (M.I); husnain3004@gmail.com (H.A)
[4]Department of Computer and Information Technology, Superior University, Lahore 54000 Pakistan; shakeel.ue.pk@gmail.com (S.A); ali.maths72@gmail.com (M.A)
[5]Department of software engineering, Gold Campus, Superior University, Lahore 54000 Pakistan, developersai643@gmail.com (M.I)
* Correspondence Author: farhan32748@gmail.com

Abstract
Perovskite solar cells (PSCs) have attracted much attention due to their good optical absorption and favorable electrical properties. While lead-based PSCs have demonstrated efficiencies up to 26.1%, the toxicity of lead has raised concerns for serious environmental and health impacts. As a result, tin-based perovskites have emerged as a promising solution as a lead-free alternative, albeit one with limited practical application due to stability problems and high defect densities. In this work, heterojunction tin-based perovskite $MASnI_3$ as the absorber layer was the solar cell numerically designed and optimized by SCAPS-1D simulation tool. A parametric study has been performed in which the thickness of the absorber, the band gap, the density of defects, the concentration of doping and operating temperature of the absorber has been varied to conduct a detailed parametric analysis. The proposed device after some optimization was 24.18% power conversion efficiency, 0.9323 V open circuit voltage, 30.836 mA/cm^2 short circuit current density and fill factor of 84.10%. The results show a dramatic decrease in recombination losses, particularly Shockley-Read-Hall recombination. These results show that tin-based perovskite solar cells can be used as efficient, cost-effective and environmentally friendly alternative to lead-based devices, which is a good basis for future experimental development.

Keywords: Lead-free, Tin-based, Perovskite solar cells, SCAPs-1D Simulation and Performance optimization.

1. INTRODUCTION

Due to the growth in population and improvement of the living standards, there is an increment in the demand of electricity to operate the appliances in the homes. The best approach to this is to shift to renewable energy sources like hydro-power, wind, and solar energy sources in order to reduce pollution as a measure to combat the problem of global warming. However, one of the major problems that have been linked to renewable energy is that it needs specialized facilities as compared to using non-renewable energies like natural gas, coal and oil [1]. Luckily, equatorial areas, which require a lot of electricity to maintain high standards of living are especially conducive to solar energy harvesting. These regions have regular sun rays throughout the year, and solar power can be a very feasible solution. The daily energy that is supplied by solar radiation is more than the annual energy that the world uses [2].

The first perovskite solar cells were introduced in 2009, but the first solar cells had a low power conversion efficiency of about 3.8%. This poor performance was largely due to instability by the liquid electrolyte that caused both the electrode and the layer of perovskite absorber to dissolve as it was operated [1]. In 2012, major advancements took place and researchers reported a stabilized efficiency of 9.7% over 500 hours, which has given rise to wide interest in perovskite solar cell (PSC) technology. Figure 1 depicts a typical architecture of PSC. In this type a transparent conducting electrode (usually indium tin oxide (ITO) or fluorine-doped tin oxide (FTO)) is deposited on a substrate of glass, and then an electron transport layer (ETL). When the perovskite absorber is illuminated it produces charge carriers selectively transfers to the ETL and a metallic top contact layer is used together with the hole transport layer (HTL) to make up the device. The contact between the metal contact and the transparent electrode forms the external circuit. The gradual improvement of the efficiency of each functional layer has been essential in improving the general effectiveness of the device. Specifically, the ETL enables

efficient extraction of electrons and inhibits charge recombination, which enhances the functioning of the device [2 - 4]. It has been found to require the use of a sufficiently thick TiO2 layer, including a mesoporous structure to occupy the interfacial voids; thinness causes the layer to be unproductive and highly resistive to shunt. Better interfacial quality reduces recombination losses and decreases ETL resistance so that a more effective electron transport can be achieved and power conversion efficiency is enhanced. The device layers are deposited using various fabrication methods such as spin coating, thermal evaporation and spray pyrolysis. Moreover, it has investigated compositional engineering of perovskite materials to improve the open-circuit voltage (Voc) and minimize energy loss over a wider spectral range [5,6]. The increased light absorption leads to an increase in the amount of charge-carrier generated, Voc, and overall energy output.

The separation of energy between the highest occupied and least unoccupied order of the molecules (the HOMO and LUMO) is the bandgap. High temperature liquid HTLs such as the CuSn, Spiro-bifluorene (Spiro-OMeTAD) are also prevalent. Salt and oxygen (O2) are also similar to these HTLs in their action [7, 8]. The conductivity of Spiro-OMeTAD is increased by doping because of its low density of charge. A heterojunction with a thin intrinsic HTL reduces the electron recombination and increases the current density of short circuit (JSC). The most preferred metal electrode is still gold (Au) although other metals may be adopted depending on the nature of the cell structure.

The task of this work is to analyze microstructural features, i.e. the thickness and the grain size distribution in Perovskite layers used in solar cells that have been made in the form of Figure 1. Moreover, assess the chemical structure, thickness, and diameter of the particles as well as the roughness on the surface of the Perovskite and establish a correlation among the electronic characteristics of the syntactic samples. To determine the variations in the efficiency of the solar panels and solar cells in converting solar energy, we can use a solar simulator. The purpose of the test is to measure the existing voltage attributes. It is also to be the case with the research of Perovskite solar cells since it is related to the composition and production process. Photoelectric activity is highly significant in study of photoluminescence (PL) and electroluminescence (EL) [9]. It is possible to enhance power conversion efficiency (PCE) to over 18 percent.

Figure 1. illustrates the arrangement of a perovskite solar cell (PSC)

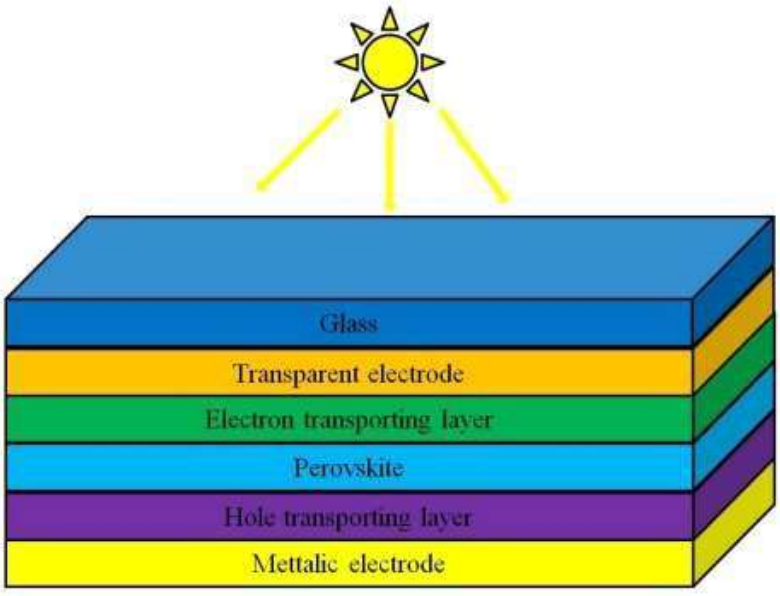

2. METHODOLOGY

This part will include a substantial amount of information as to how the device was constructed and the specific settings that were used in the simulation. Three architecture planar (n-i-p), inverted (p-i-n), and mesoporous architecture are commonly used in developing Perovskite design. A heterojunction structure of the device was used, and CH3NH3SnI3 as the active material in the current paper. The stack consisted of FTO, ZnO, CH3 NH3, CuSCN, and Au. The device was measured using the solar cell simulator SCAP-1D, which is a device that was developed at the University of Poisson and relies on the continuity equations and the Poisson equation. The simulation of device behavior is solved numerically by solving a coupled system of fundamental semiconductor equations, i.e., the Poisson equation [25], the equations of continuity of electron transport [26] and the equations of continuity of hole transport [27]. By solving these equations, it is possible to significantly analyze the internal electrical characteristics of the solar cell (e.g., current density-voltage characteristics, band energy alignment,

spectral quantum efficiency, and so on). Essential photovoltaic performance characteristics are then obtained using the simulated output characteristics that include the power conversion efficiency, fill factor, open-circuit voltage, and short-circuit current.

$$\frac{d}{dt}\left(-e(t)\frac{d\psi}{dt}\right) = q[p(t) + N_D^+(t) - N_A^-(t) + p_t(t) - n_t(t)] \quad (1)$$

$$\frac{dP_n}{dy} = G_p - P_n - \frac{p_{n0}}{\tau_p} + n_p\mu_p\frac{d\xi}{dy} + \mu_p\frac{\xi dP_n}{dy} + D_p\frac{d^2P_n}{dy^2} \quad (2)$$

$$\frac{dn_p}{dy} = G_n - n_p - \frac{np_0}{\tau_p} + n_p\mu_n\frac{d\xi}{dy} + \mu_n\frac{\xi dP_n}{dy} + D_p\frac{d^2P_n}{dy^2} \quad (3)$$

The parameters that explain the various components of the system are the rate of electron generation, the electron lifetime, the hole lifetime, diffusion coefficient, the elementary charge, the electron potential, the electron velocity, the hole velocity, the concentration of ionized acceptors, trapped electrons, and free electrons, the energy of ionized donors, the strength of the electric field and the thickness of the device (represented by x). Figure 3 depicts the general structure of the device and all the intermediary layers. The energy level diagrams were drawn by the observation of the tracks of the produced electrons and holes by the absorber layer. Then, experimental identification of the position of the valence band (VB) and the conduction band (CB) of each individual layer were conducted.

As depicted by Figure 3, the perovskite solar cell has been modeled in the form of a multilayer setup with six functional layers. Titanium dioxide (TiO2) is used as the electron transport medium whereas methyl ammonium tin iodide (MASnI3) is used as the light-absorbing layer. On the light side, a fluorine-doped tin oxide (FTO) is used to form electrical contacts and on the back side, gold (Au) is used, thus permitting the collection of charge and connection to external-circuit components. The device is essentially characterized by the FTO and ETL interfaces, ETL and perovskite interfaces, and perovskite and hole transport layer interfaces. All simulations and data of the results were achieved in standard test conditions, which are a pressure of 1.5G of mass air, a temperature 300K, and a light intensity 1000W/m2.

2.1. CuSCN-oriented HTL

Copper thiocyanate (CuSCN) has a large amount of literature on its use as a hole-transport material in organic and hybrid optoelectronics. But its polymer nature coupled with coordination renders the conventional soluble fabrication difficult. Consequently, deposition normally depends on sulfur based solvent systems, which react well with copper and allow some process ability of CuSCN thin films. Our curative suggestion would be a simple wash of the CuSCN HTL with such an anti-solvent as acetone or tetrahydrofuran and in the process inhibit the undesired solvent-copper interactions. It has been experimentally validated to improve the performance of organic light-emitting diodes (OLEDs) and CuSCN based solar cells as an HTL, namely, through an increase in the short-circuit current density (JSC) and fill factor of an organic photovoltaic (OPV) system. The untreated CuSCN optoelectronic PV devices enhance its average power-conversion efficiency (PCE) by 9.16 and 9.25 percent under the influence of the rinsing acetone and tetrahydrofuran respectively. In addition, the external quantum efficiency (EQE) of the OLEDs utilizing a CuSCN HTL is 8.2 5.2tetrahydrofuran treatment to 8.2. Thus, the inclusion of an anti-solvent rinse methodology is an effective and convenient methodological addition to the solution processing of CuSCN in diverse organic optoelectronic devices and will tend to add measurable changes to the behave-success of the devices to the industrial practice. The following task in work is the further optimization of the anti-solvent treatment protocol, the control over the investigation of other anti-solvent chemistries and the overall assessment of their compatibility with a variety of devices arrangements. Such studies will be necessary in the transferring enhancements of them at the laboratory levels to powerful and manufactural manufacturing levels. As far as the use of perovskite solar cells is concerned, the existing production process of the CuSCN HTLs on the indium -doped tin oxide (ITO) products not only is resource-intensive but costly in time. We also suggest the use of monoethanolamine (MEA) as the sole solvent in the deposition of CuSCN in which we employ the two-step spin-coating followed by the low-temperature annealing. The approach reduces the cost of production and cycle time and does not sacrifice the quality of HTL. The surface morphology, crystalline structure, and optical properties of MEA-processed CuSCN layer were identified using the assistance of the scanning electron microscopy (SEM), X-ray diffraction (XRD) [36], and ultraviolet-visible spectroscopy (UV-Vis), respectively. Current voltage (I-V) was used to measure the sheet resistivity and it was observed that the optimum annealing temperature was 100 degree resulting in a highly ordered film of conductivity of 77.30 S m -1. The findings indicate that MEA has the potential to replace costly solvents and preserve electrical and morphological characteristics that high-efficiency HTLs must have. With such a new way of production of CuSCN HTL layers,

the way to the cost-effective and efficient production of these layers becomes open with the help of the appropriate solvent system and annealing parameters. The implications of these findings to the market of perovskite solar cells are significant because the simplified process will reduce the cost of producing and enable mass production. It appears that the MEA route can be used to produce HTL layers on a large-scale basis, and this will greatly lower the price of production, which in its turn will multiply the commercial availability of perovskite solar cells.
It requires more research on optimization and scalability to facilitate reproduction of the findings on industrial basis. In addition, long-term stability tests and other compatibility tests with other constituent materials will be required to conclude the entire validity of the practical applicability of MEA-based CuSCN HTLs.

2.2. ETL based on ZnO

Perovskite solar cells are also regarded as a prospective technology in the next-generation photovoltaic technology due to their ability to be produced at relatively low temperatures and their ability to transport charge effectively. Although these have been beneficial, the chemical instability of perovskite absorbers at the interface with ZnO has limited their scalability and led to poor performance of the devices. In order to overcome this drawback, a two-layer electron transport device with yttrium-doped TiO2 and vanadium-doped ZnO has been suggested. The concomitant application of Y-doped TiO2 and V-doped ZnO as electron transport layers has shown a significant improvement in the working efficiency of perovskite solar cells at optimized dopant concentrations between the two.
The power conversion efficiency (PCE) of the devices utilizing the (V ZnO/yti)/ bilayer ETL was found to be 15.1% as opposed to 9.4% of the PCE of ZnO-only ETLs. The parameters used are F Fill factor 74 0, O Circuit voltage 923 mV, and S Short circuit current density 22 mA cm -1. The enhanced electron transport that the bilayer architecture provides explains a bright future of wider application of ZnO-based ETLs, provided that the stability problems that have hitherto restrained their application are addressed.
The implementation of this bilayer approach increases the viable application scope of ZnO ETLs, provided that the instability is reduced. The further implementation of perovskite solar cells is expected in the case of concerted efforts aimed at the activation and optimization of the (V:ZnO)/Y-doped TiO2 bilayer ETL to be used in the industrial scale production. This two-layer ETL system can provide a feasible remedy to the destabilization of perovskite layers coupled with ZnO, thus enabling commercial implementation [37].

2.3. FTO Glass Coating

Organic and inorganic Perovskite solar cells on a large scale have a future potential of being a low-cost alternative to photovoltaic systems. However, all such cells are not immune to damage and other issues along with the toxicity of the lead, on which they are crafted. Therefore, there is a need to identify effective ways of discarding the PSC waste and recycling of the components. The research paper suggests the systematic method of reducing the high cost of fabrication of mesoporous planar perovskite solar cells by enabling the use of the fluorine-doped tin oxide (FTO)-coated glass substrate through a controlled step-by-step process of layer-by-layer removal. The approach will enable the preservation of useful elements, such as gold contacts and Spiro-OMeTAD, without losing their chemical properties, as every functional layer can be removed sequentially. Therefore, it will be easier to recycle the substance. In addition, it will ensure that it will segregate the toxic Pb element but will not pollute the other materials. After removing all the layers, the FTO conductive glass may be reused and used in many ways not related to photovoltaics. It was determined that there were not many differences between electrical, morphological and physical properties of recycled FTO glasses and commercial glasses. It is a witness of the efficiency of the recycling strategy towards retrieving the substrate without compromising its physicochemical properties.
The suggested program of recovery of PSC surplus gives a viable and green approach of managing PSC waste when it is no longer useful to it [37]. This strategy is effective by allowing the use of invaluable elements and reducing the risk of lead poisoning of PSC technology by the degradation and poisonous nature of the technology. Considering the expected-value, the recycling of the FTO-coated glass substrates will greatly lower the expenditure spent on the production of fresh materials of substrates in PSCs. This reduces the energy cost to the environment involved in the mining and production of raw materials and makes overall solar equipment cost-effective. Considering this recycling method means a huge boost in the sustainability of the solar energy industry [38]. It encourages the reuse of resources of value and minimizes waste, and this guides toward the circular economy. In future projects of research and development this recycling should be enhanced and expanded as a high priority of the new projects. The following measures will involve examining other applications to recycled FTO conductive glass beyond its current scope of interest in numerous industries. solar energy. This method of recycling will also be supported by the long-term experiments that will be used to prove viability and functionality of the recycled parts in the real life condition.
To have a viable recycling process, the fluorine-doped tin oxide (FTO) coating on the glass substrate should not be polluted. To ensure that the recycling process adds to the restoration of high- quality FTO glass without changing the crystalline phase or damaging the conductive oxide coating X-ray diffraction (XRD) of the recycled samples was compared to the XRD of the untreated reference substrates. The fact that the diffract grams of the

recycled and pure FTO glass are almost similar supports the validity of the recycling method. In particular, the number of additional diffraction peaks or peak shifts was not observed, which means that the crystal structure and the conductive layer of oxide were not destroyed. Moreover, the XRD outcomes showed that the intensity of freshly prepared FTO was lower as compared to the intensity of the recycled samples [38]. This difference is described by differences in crystallite size distribution since the entire width at half maximum of diffraction peaks is directly proportional to the size of crystallite.

The decrease in full width at half maximum is accompanied by an increase in area of the peak, which goes hand in hand with an increase in the size of crystallites. This difference in the intensity of the peaks could also be explained by diffractometer-related influences, e.g., by the difference in exposure time per phase, or by the change in binary oxidation states caused by high-temperature annealing. These factors are essential, with the XRD pattern of FTO still having a TiO2 mesoporous layer being investigated to be able to unambiguously prove the lack of TiO2 in the recycled substrate. Further indications of the purity of the recycled substrate are represented by the absence of discernible TiO2 peaks in the phase composition.

2.4. SCAPS-ID

The solar devices can be modelled and analyzed with high accuracy using the simulation program. Specifically, one would focus on SCAPS 1D which is a simulation program that does not allow any other input but the rear. The proposed fix is the enhancement of SCAPS 1D software that will enable the back to be specified as one of the input parameters. In this regard, the simulation and analysis of photovoltaic devices will be improved. The recent addition on the SCAPS-1D modeling platform adds a more realistic and realistic modeling platform to the researchers and device designers [39]. The software can also be optimized and evaluated in this way more efficiently, with the backside interface as an added input parameter, thus making more accurate predictions regarding the actual performance of the device. The effect of such augmentation is significant since it not only increases the range of SCAPS-1D but also allows the researchers to understand more about the optical and electrical characteristics of the materials. It, therefore, promotes science and streamlines solar device optimization. The remaining processes involve incorporating the improvements to be made in the existing SCAPS system, which is compatible with Windows. Besides, the readily available documentation and guidelines must be provided in an attempt to ensure that the enhanced SCAPS-1D program is accessible and easily used. Simulation of the structural properties of semiconductors is done with SCAPS-1D. Regarding process simulation, Figure 2, depicts the process that should be followed in designing and simulating the proposed system.

Figure 2. Procedure for constructing and simulating a solar cell using SCAPs-1D

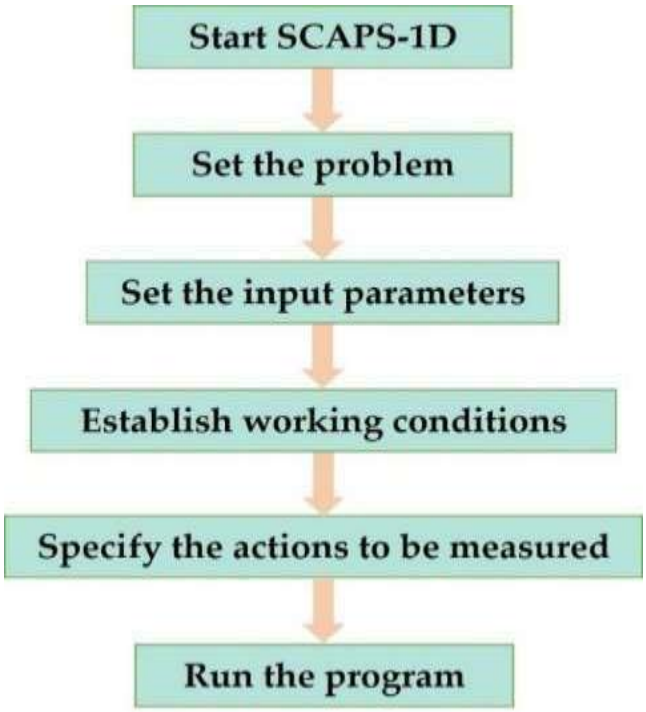

Figure 3. SCAPS 3.3.09 Action Panel

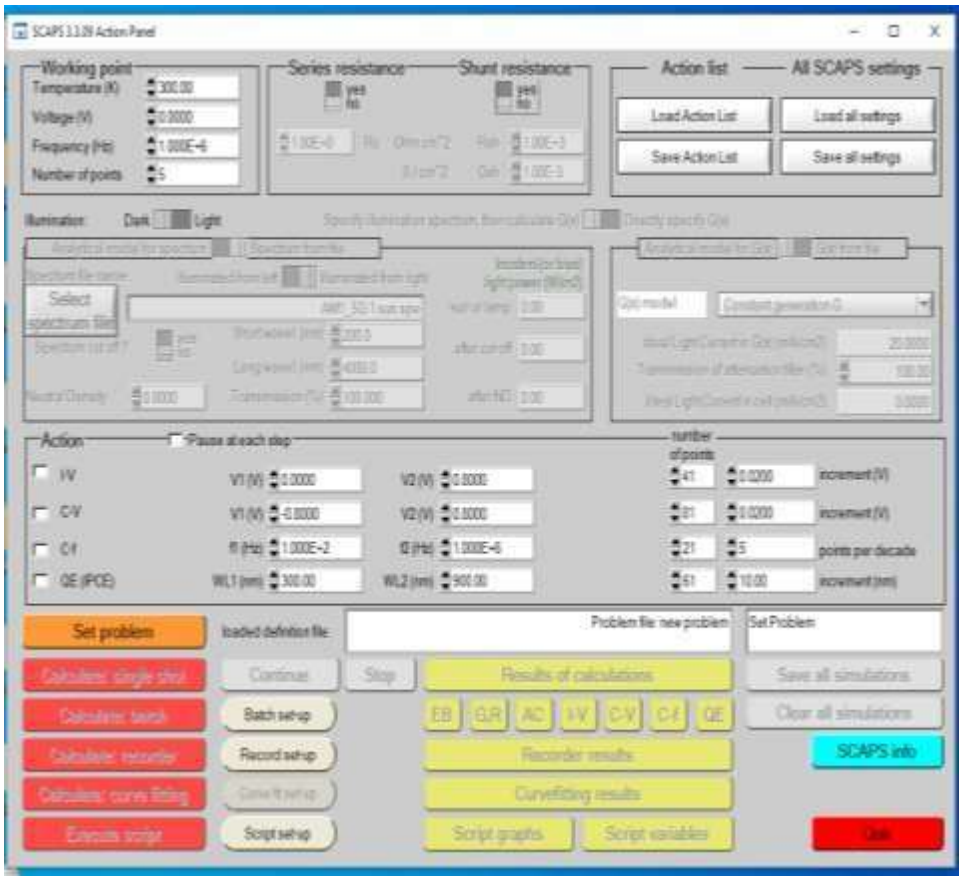

Figure 4. The complete stack of functional layers is arranged according to an n – i – p planar device architecture

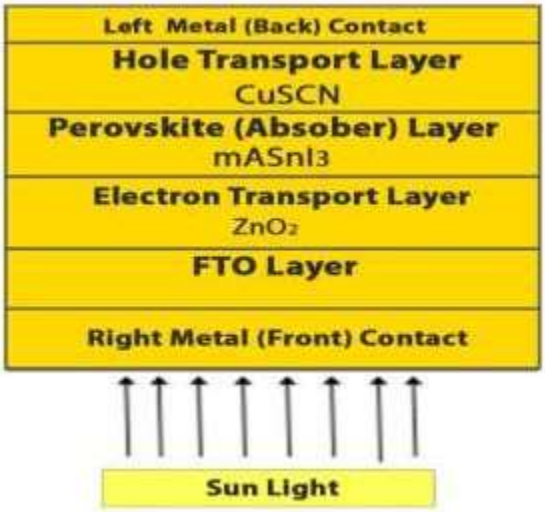

Figure 5. Energy-level band alignment of the perovskite solar cell device.

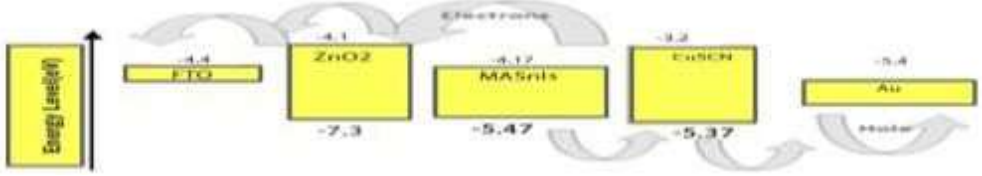

Table 1. Simulation input parameters corresponding to each functional layer of the perovskite solar cell.

Variables	FTO 1Glass	ZnO	CuSCN	$CH_3NH_3SnI_3$
Thickness 1(nm)	400	1 1 1 1 1 150	1 1 1150	1 1 1 1 1 1 1 1 1 1 1 1650
Electron 1affinity 1(eV)	4.000	4.200	2.200	4.170
Bandgap 1(eV)	3.500	3.260	3.400	1.350
CB 1effective 1density 1of 1state 1N 1c 1($1cm^{-3}$)	2.200 $1e^{18}$	2.20 $1e^{18}$	1.700 $1e^{19}$	2.20 $1e^{18}$
Dielectric 1permittivity 1(εr)	9.00	10.00	10.00	8.200
VB 1effective 1density 1of 1state 1NV 1($1cm^{-3}$)	1.8 $1e^{18}$	1.80 $1e^{18}$	2.50 $1e^{21}$	1.800 $1e^{18}$
Hole 1mobility 1μp 1(cm^2/Vs)	1.0 $1e^{1}$	1.00 $1e^{1}$	1.00 $1e^{-1}$	3.0 $1e^{2}$
Electron 1mobility 1μe 1(cm^2/Vs)	2.0 $1e^{1}$	2.00 1 $1e^{1}$	1.00 $1e^{-4}$	2.0 $1e^{3}$
Thermal 1velocity 1 1of 1Hole 1cm/s	1.0 $1e^{7}$	1.0 $1e^{7}$	1.0 $1e^{7}$	1.0 $1e^{7}$
Thermal 1velocity 1of 1Electron 1 1 1cm/s	1.0 $1e^{7}$	1.0 $1e^{7}$	1.0 $1e^{7}$	1.0 $1e^{7}$
Acceptor 1density 1NA(cm^{-3})	0.00 $1e^{0}$	0.00 $1e^{0}$	1.0 $1e^{18}$	1.0 $1e^{18}$
Donor 1density 1ND(cm^{-3})	1.0 $1e^{19}$	1.0 $1e^{17}$	0.0 $1e^{0}$	0.0 $1e^{18}$
Density 1of 1Defect 1Nt 1($1cm^{3}$)	1.0 $1e^{15}$	1.0 $1e^{15}$	1.0 $1e^{15}$	1.0 $1e^{15}$

Table 2. Parametric estimation connections and issues.

Variables	$ZnO_2/CH_3NH_3SnI_3$	FTO/ZnO_2	$ZnO_2/CH_3NH_3SnI_3$	$CH_3NH_3SnI_3/CuSCN$
Defect 1type	Neutral 1(1N)	Neutral 1(1N)	Neutral 1 1(1N)	Neutral 1 1(1N)
Capture 1cross-section 1Hole Σ_p 1(cm^2)	1 $1e^{-15}$	1 $1e^{16}$	1 $1e^{16}$	1 $1e^{16}$
Capture 1cross-section 1Electron $\Sigma_1 n$ 1(cm^2)	1 $1e^{-15}$	1 $1e^{16}$	1 $1e^{16}$	1 $1e^{16}$
The 1energy 1levelconcerning 1Reference E_v 1(eV)	0.600	0.600	0.600	0.600
Utilization 1Energy	Single	Single	Single	Single
Density 1of 1Defect N $1_{t\,1}$($1cm^{-3}$)	1.0 $1e^{16}$	1.0 $1e^{16}$	1.0 $1e^{16}$	1.0 $1e^{16}$

Energy 1factors	00	00	00	00

3. RESULT AND DISCUSSION

3.1 Influence of Absorber Layer Thickness on Device Performance Parameters

The absorber layer plays a critical role in determining the overall functionality of perovskite solar cells. Its thickness must be carefully optimized to ensure efficient light harvesting while maintaining sufficient charge-carrier diffusion. In this study, the influence of absorber thickness on device performance was systematically investigated over a thickness range of 300 nm to 1000 nm. The following table depicts the results of the computations. As is observable in the table and graph, the introduction of the thickness of the material caused significant changes in the values of Jsc and PCE, thus showing a lot of improvement. The gain was 300nm-900nm due to the increase in the absorption coefficient as it was earlier found out in some research [28] provided.

A further increase in the thickness of the absorber layer results in a measurably lower open-circuit voltage (Voc), which is explained by an increase that happens in the recombination of charge-carriers at the absorber bulk and interfacial sites [29]. The same downward trend is followed by the fill factor as the thickness is increased, which is mainly because of increment in the series resistance within the device. The thicker the absorber layer, the retarded charge transport, which is averse to the overall performance of the device. The power conversion efficiency is at a higher value at lower values of thickness close to 300 nm but it shows a sharp drop as the thickness is close to 800nm.

This tendency is closely connected with changes in the carrier diffusion length. Reduced carrier transport thickness will assist in increased power conversion efficiency at lower thicknesses (300-800 nm). After this point, the diffusion length will reduce significantly, and hence recombination will cause greater losses and eventually the efficiency will be reduced [30]. The excessive absorber thickness is then counterproductive as it reduces the extraction of charges.

The performance measures of various absorber thicknesses in terms of the device were summarized in the table below. The open-circuit voltage shows a slow rise with the increase in thickness (between 350 nm and 600 nm) and then it rapidly decreases and is near negligible values at 600 nm and above. The current density of the short-circuit (Jsc) exhibits a small effect on the thickness with varying values of around $26.39\ mA\ cm^{-2}\ to\ 30.83\ mA\ cm^{-2}$ and then it becomes constant. The fill factor is slightly constant over the thickness range under evaluation, typically ranging between 75%-85%. It is worth noting that at the absorber thickness of 600 nm, the power conversion efficiency peaks at 24.18% and the power conversion efficiency ranges between 18.03% and 24.18% at the different thicknesses of the absorber that have been studied. These results demonstrate that there is an optimal absorber thickness to maximize photovoltaic performance and it is important to undertake further research on the physical processes that control the thickness dependence in efficiency maximization.

Table 3. Impact of thickness on performance characteristics.

Thickness 1 (nm) 1of 1CH3NH3SnI3	Jsc 1 1(mAcm^{-2})	Voc 1 1(V)	FF 1 (%)	PCE (%)
300	26.36	0.9226	84.21	20.58
350	27.57	0.9238	84.18	21.54
400	28.48	0.9238	84.15	22.28
450	29.19	0.9289	84.13	22.85
500	29.74	0.9302	84.12	23.30
550	30.18	0.9305	84.11	23.65
600	30.54	0.9310	84.10	23.94
650	30.83	0.9359	84.10	24.18
700	31.07	0.9376	1 1 1 184.09	24.37
750	31.27	0.9385	84.09	24.54
800	31.45	0.9388	84.08	24.68
850	31.59	0.9391	84.08	24.80
900	31.72	0.9394	84.08	24.90
1000	31.93	0.9398	84.07	25.08

Figure 6. Impact of Thickness on performance parameters of CH3NH3SnI3 VOC (v) Jsc (mA/cm2), PCE (%) , FF (%)

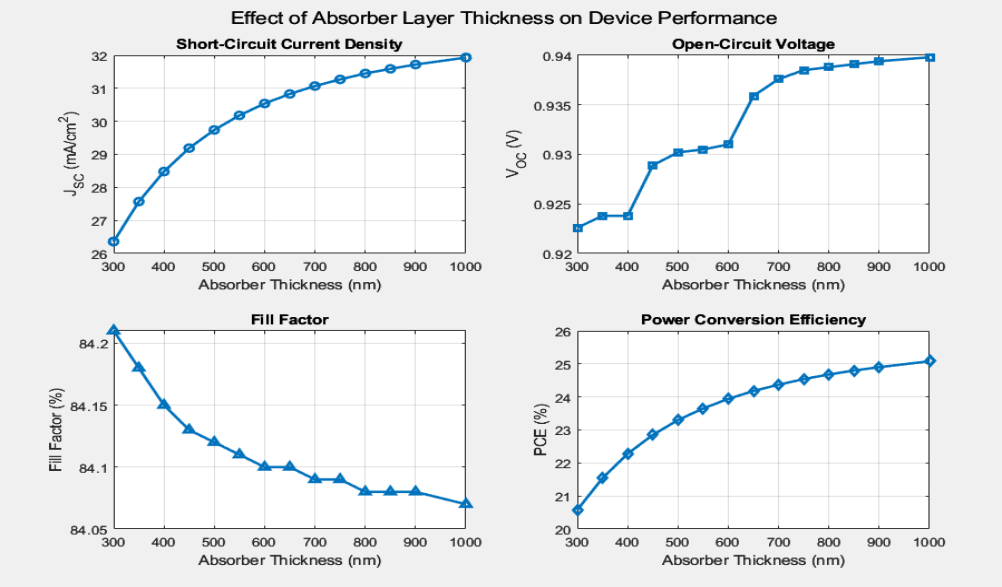

3.2 Effect of Absorber Layer Acceptor Doping Concentration (N_a) on Device Performance Parameters

A high concentration of hole carriers in the absorber layer can cause degradation to the performance of perovskite solar cells. Tin-based perovskites are highly unstable at ambient temperature, with the Sn 2 + oxidation state easily reduced to Sn 4 + under the influence of self-p -type dopants. The oxidative change of the tin component has a negative impact on the efficiency of the device. Takashi and his colleagues studied the effect of the concentration of holes by changing the density of the acceptors and established that a density of 1.0 e10 cm-3 generated significant variations in the key performance indicators [32].

With a higher concentration of the acceptor in the layer of the absorber, the open-circuit voltage (Voc) will increase, and it can be explained by the fact that the acceptor quasi-Fermi level will decrease and the built-in potential (Vbi) will increase. Nonetheless, also, increased dopant concentrations lead to a minor decrease in short-circuit current density (Jsc), which is mainly caused by an increased probability of recombining charge carriers. It is worth noting that the fill factor, as well as the power conversion efficiency, is significantly enhanced when the concentration of acceptors.This increase in performance can be linked to long carrier diffusion lengths and reduced resistive losses in the perovskite matrix, which in combination with one another lead to high efficiency of the device.

Table 4. Influence of Absorber Layer Acceptor Density on Photovoltaic Performance

1Density 1of 1acceptor 1(N_A 1cm^{-3}) 1 1 1 1	Voc(V)	JSC 1(mAcm^{-2})	FF 1(%)	Power 1conversion 1efficiency 1(%)
1e^{13}	0.80	30.04	77.15	18.67
1e^{14}	0.81	30.05	77.16	18.66
1e^{15}	0.82	30.05	77.34	18.79
1e^{16}	0.84	29.99	79.24	20.02

Figure 7. Impact on doping concentration (NA) of CH3NH3SnI3, VOC (v), Jsc (mA/cm2)

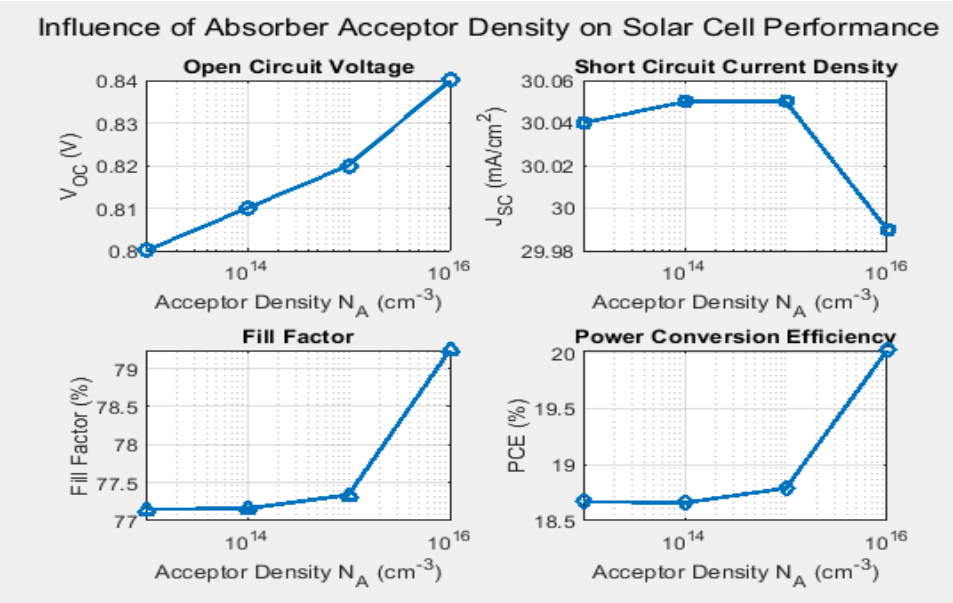

3.3 Impact of Absorber Layer Defect Density on Device Performance Measures

Tin perovskites are extremely imperfect and the degree of imperfections defines greatly the quality of performance and the stability of the layer of absorber. These defect states may originate within the bulk of the perovskite film or arise at interfaces between the absorber and adjacent charge-transport layers in PSC. Interfacial defects are particularly significant, as they tend to accumulate at layer boundaries and introduce shallow electronic states within the perovskite band structure, thereby affecting charge transport and recombination behavior.

The load of defects in the absorber layer is a decisive variable of diffusion length of charge carriers in perovskite substances. An increase in the defects that are extended concentration is associated with a reduction in carrier diffusion length. The performance measures became independent of the defect density since the attainment of a higher defect density after an adjustment in the defect density that ranged between $1\ e^{13}\ to\ 1\ e^{19}\ cm^{-3}$. The received data is condensed in Table [34]. All of the key photovoltaic performance metrics, including open-circuit voltage (Voc), short-circuit current density (Jsc), fill factor (FF), and power conversion efficiency (PCE), uniformly deteriorate with increased defect density in the absorber material. The cause of this degradation is largely due to the diffusion length of charge-carriers decreasing due to the increased non-radiative recombination in the absorber. At the point at which the defect concentration is around $1.0 \times 10^{19} cm^{-3}$, there are pronounced performance losses in the device and it can be said to be electrically unstable.

The effect of the density of the defects on the absorber layer can be explained with the help of Shockley-Read-Hall (SRH) recombination model. There are normally three recombination processes that perovskites constitute through radiative processes, non-radiative processes and Auger recombination. It is primarily due to the high concentration of the defects in the absorber layer that non-radiative (SRH) recombination currents can be influenced. Absorber defect density grows with the rate of recombination and thus, it forms part of the issues that lead to poor performance of perovskite solar cells.

The conduction band offset (CBO) of the interface of the absorber and the buffer layer is tightly associated with the creation of interfacial defect states, that have a profound effect on the overall device performance. In order to prevent the formation of such defects, it is suggested to design a positive CBO by placing appropriate interfacial layers between the absorber and the other layers that transport charge. Concentration of defects at the interface of the perovskite absorber and electron transport layer (ETL) tends to be high as compared to the interface of the absorber/hole transport layer (HTL). Besides, the sensitivity of the carrier diffusion characteristic in the absorber can be assessed quantitatively through analytical expressions, which link length of diffusion to the density of defects existing in the absorber material.

$$L_D = \sqrt{D\tau} \qquad (4)$$

Carrier mobilities of electrons and holes are proportional to diffusion coefficients respectively. The high density of defects in the absorber layer is thus likely to inhibit the carrier diffusion length, and as a result, it impairs the functionality of perovskite-based devices. To the extent that the density of the defects in the absorber is decreased to about 1 x 1013 cm -1 recombination currents can be cut by a significant factor and carrier diffusion lengths get considerably longer and the overall performance of the device is significantly improved.

Table 5. Impact of defect density on performance of parameters

Defect 1of 1density 1 1(cm^{-3})	JSC(1mAcm^{-3})	VOC(V)	FF 1(%)	PCE 1 1(%)
1e^{13}	30.06	0.85	83.30	21.38
1e^{14}	30.06	0.85	83.26	21.36
1e^{15}	30.06	0.85	82.86	21.22
1e^{16}	30.03	0.83	80.27	20.24
1e^{17}	30.01	0.77	75.68	17.64
1e^{18}	29.74	0.67	70.24	14.15
1e^{19}	27.11	0.56	55.98	8.51

Figure 8. CH3NH3SnI3 Defects density(NA) and VOC , CH3NH3SnI3 Defects density(NA) and Jsc

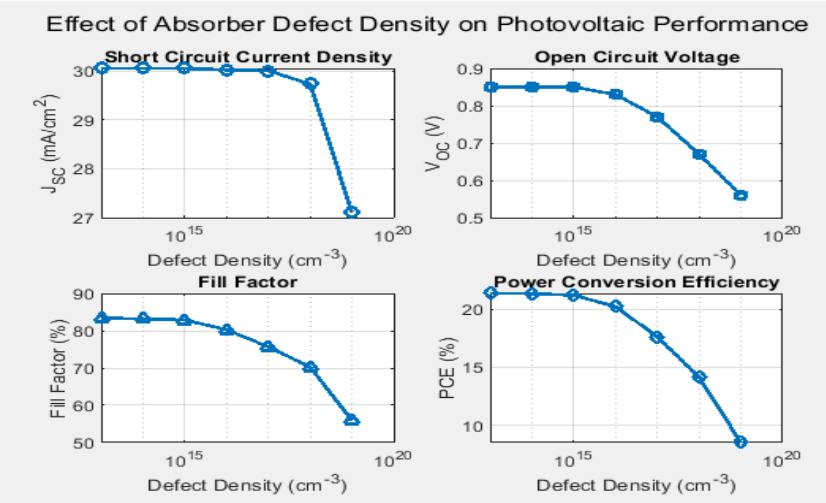

3.4 Analysis of Interfacial Defect States at the ETL/Perovskite

The above part has clearly investigated the effect of the defect density of the absorber-layer and given tentative conclusions on the degradation of the performance of perovskite photovoltaics. The modelling and design of MASnI3 based perovskites was done using the n-i-p planar architecture. In this planar design, carrier mobility on a hole basis in the absorber layer, which carries the carriers to the corresponding hole-transport layer (HTL) and electrodes, is higher than that of electrons. Therefore, planar designs analysis is critical in explaining interface defects at the ETL/perovskite junction, where high recombination currents are recorded.

The interfacial defects between the ETL and the perovskite should also be assessed, as interfacial defects slow down the electron mobility towards the electrodes. The present paper has discussed the densities of interfacial defects (10 e16 1 e19 cm -2) on the key performance parameters. It was discovered during the experiments that concentration of the imperfections within the absorber had a detriment effect in the performance parameters and more defects in the interface led to a significant decrease in the entire measured parameters. The experimentally determined reduction in short circuit current density (Jsc) is attributable to higher interface rates of Shockley Read Hall (SRH) recombination current between the perovskite/ETL interface. There is also the reduced open-circuit voltage (Voc) and this reduction is associated with the increased dark saturation current that also significantly minimizes Voc. This is given as an increase in the dark saturation current that accompanies an increase in the recombination currents. Voc v reverse saturation current is represented by equation below.

$$V_{oc} = \frac{nKT}{q} ln\left(\frac{J_{sc}}{J_0} + 1\right) \qquad (5)$$

The symbols n, T, Jsc, q, Jo and VOC in the governing expression represent the diode ideality factor, the absolute temperature, the elementary charge, the reverse saturation current, the density of the short-circuit current, and the open-circuit voltage, respectively. The greater the recombination-related current, the greater the size of the reverse saturation current, and hence, the decrease in the open-circuit voltage.

Table 6. Influence of Interfacial Defect Density at the ETL/Perovskite Interface

ETL/Perovskite 1 1 Defect 1of 1density 1 1(cm^{-2})	Jsc 1 1 1 1 1 1 1 1 1 1 1 1 1 1 1 1 1 1 1 (1mAcm^{-2})	Voc 1(V)	FF 1 (%)	PCE 1 (%)
1e^{16}	30.05	0.81	77.17	18.67
1e^{17}	30.01	0.80	77.01	18.54
1e^{18}	29.73	0.78	75.43	17.69
1e^{19}	28.64	0.77	71.79	15.86

Figure 9. Impact of interfacing Defects density (NA) of ETL/CHENH3SnI3 , VOC(v) , Jsc(mA/cm2) , FF(%) , PCE(%)

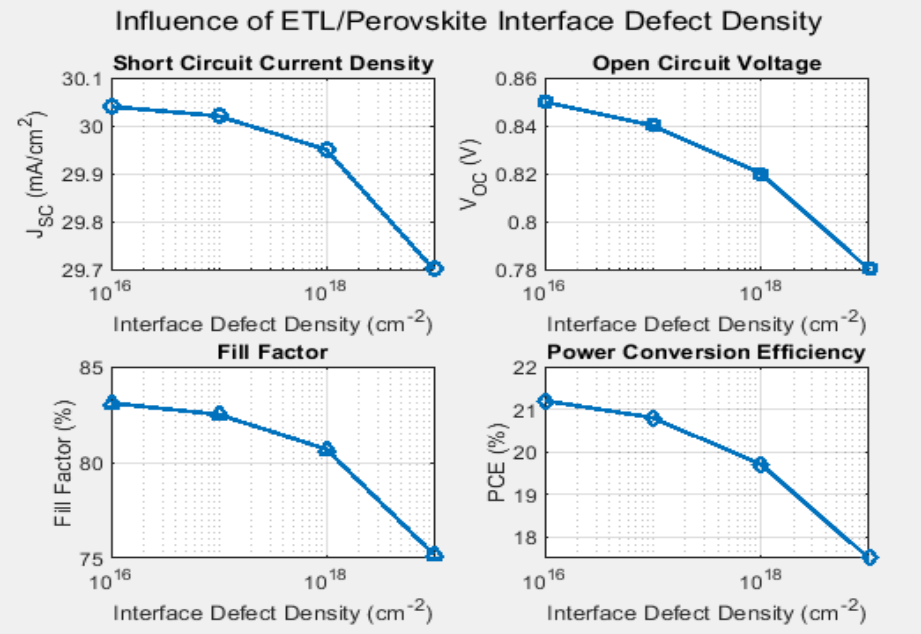

3.5. Effect of Absorber Layer Bandgap on Photovoltaic Performance Parameters

The electronic bandgap of tin-based perovskite materials is strongly dependent on their chemical composition, particularly the specific perovskite structure and the incorporated halide species. Reported bandgap values for these materials typically span from 1.30 eV to 2.15 eV [35]. In the present simulation study, the influence of bandgap variation on device performance was examined by adjusting the bandgap of the MASnI3 absorber layer within a narrower range of 1.30 eV to 1.44 eV. While this adjustment resulted in an increase in the short-circuit current density, it simultaneously caused a decline in both the fill factor and the power conversion efficiency. The single ratio that has grown which is VOC may be attributed to the subsequent rise in the band-gap energy. Band gap and VOC were directly related, the bigger the band gap the slower the radiative recombination process and consequently the large the VOC.

The presence of high band-gap values will consequently lower JSC since the amount of the electron generated in the layer of the absorber will be low. The mismatch in the band gaps between the absorber and the layer used to transport holes was the reason behind the degradation of FF. The same trends were experienced in PCE that is very dependent on the FF and thus deteriorated as the FF marketed. A band gap of 1.35 0 e V was found to give the maximum performance of the device, and this is near to the literature and previous studies [36-37-39].

Table 7: Effect of the energy band gap of performance on the absorber layer

Energy 1 1Bandgap 1(ev)	Jsc 1(mAcm^{-2})	Voc 1(V)	FF 1(%)	PCE 1(%)
1.30	31.64	0.77	75.75	18.47
1.32	31.06	0.78	76.28	18.61
1.35	30.05	0.80	77.17	18.67
1.40	28.31	0.83	78.80	18.53

1.44	26.71	0.84	70.16	18.05

Figure 10. Impact of Energy band on the CHENH3SnI3 performance parameters are Voc , Jsc , FF , PCE

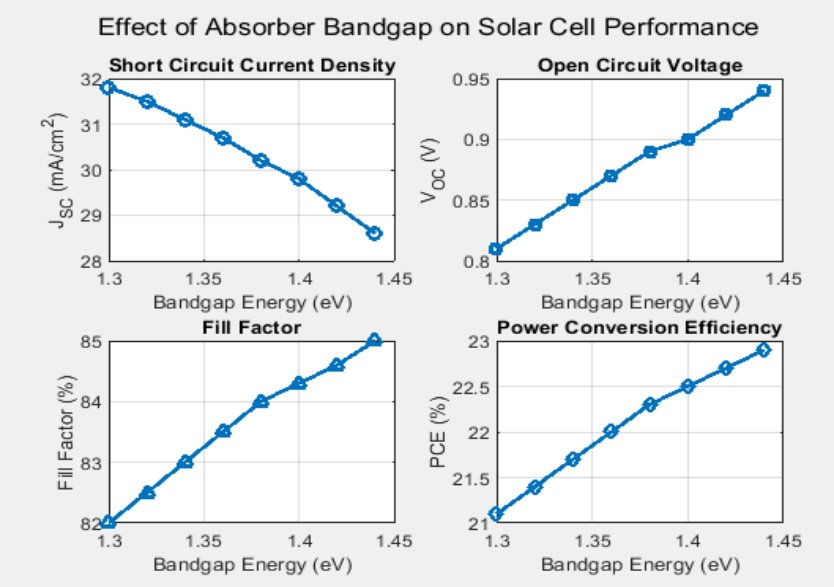

3.6. Influence of Front and Rear Metal Contacts on Device Performance Metrics

The major differences in the workability of the front and the back metallic contacts cause a significant alteration in the nature of the performance of the tin-based perovskite solar cells. The main purpose of these electrodes is to allow effective extraction of charge carriers- electrons in the electron transport layer and holes in the hole transport layer so that there is reduced carrier buildup in the device. A set of simulations was carried out to assess how the work-function values of the contact material affect the photovoltaic behavior by using front and back electrodes with systematically changed work-function values.

Published papers and literature were used to find the work energy functions of various metal contacts. These are Cu, Ag, Cu carbon-doped and Au with work functions of 4.6, 4.7, 5.0 and 5.4 electron volts, respectively. Work functions of 4.4, 4.7, and 5.03 eV were the work functions of the front metal contacts (FTO, ITO, ATO). The references were given by the user [40] and [41]. The findings indicate that the measures of performance were improved in metal contacts with more work energy functions than the ones with lower work energy functions.

High work energy functionality metal contacts increased the extraction of generated carriers towards their electrodes, and caused the improvement in performance parameters of PCE, Fill factor, and Jsc. Such a behavior is explainable by the fact that the interfacial potential barriers that charge carriers are exposed to decreases with an increase in the work functions of both metal contacts, both front and back. The surface barrier at the anode/CuSCN interface as a result can quantitatively be described in the following expression. The equation is as follows:

$$\emptyset_B = \frac{E_g}{q} + \chi - \emptyset_M \qquad (6)$$

In this analysis, parameters including the CuSCN bandgap, elementary charge (q), electron affinity (χ), and the anode work function (M) were taken into account. For the device configuration used in the simulations, gold (Au) was selected as the rear electrode, while fluorine-doped tin oxide (FTO) served as the front contact. This electrode combination resulted in enhanced device performance, primarily due to more efficient charge-carrier extraction and a further reduction in interfacial potential barriers.

Table 8. Effect of Metal on contacts with different work energy functions

1Work 1Energy 1Function 1(ev)	JSC 1(mAcm^{-2})	VOC 1(V)	FF 1(%)	PCE 1(%)
Cu 1(4.6)	29.98	0.71	54.51	11.70
Cu 1doped 1with 1Carbon 1(5.0)	30.00	0.80	77.16	18.64
Au 1(5.4)	30.05	0.80	77.17	18.67
Ag 1(4.7)	29.99	0.79	60.76	14.43

Work 1Energy 1Function 1(ev)	J_{sc} 1($mAcm^{-2}$)	V_{oc} 1(V)	FF 1(%)	PCE 1(%)
1 1 1 1 1 1 1 1FTO 1(4.4)	30.05	0.80	77.17	18.67
ATO 1(5.03)	30.04	0.80	74.23	17.95
ITO 1(4.7)	30.05	0.80	77.13	18.66

Figure 11. Work energy functions on Device Performance Parameters

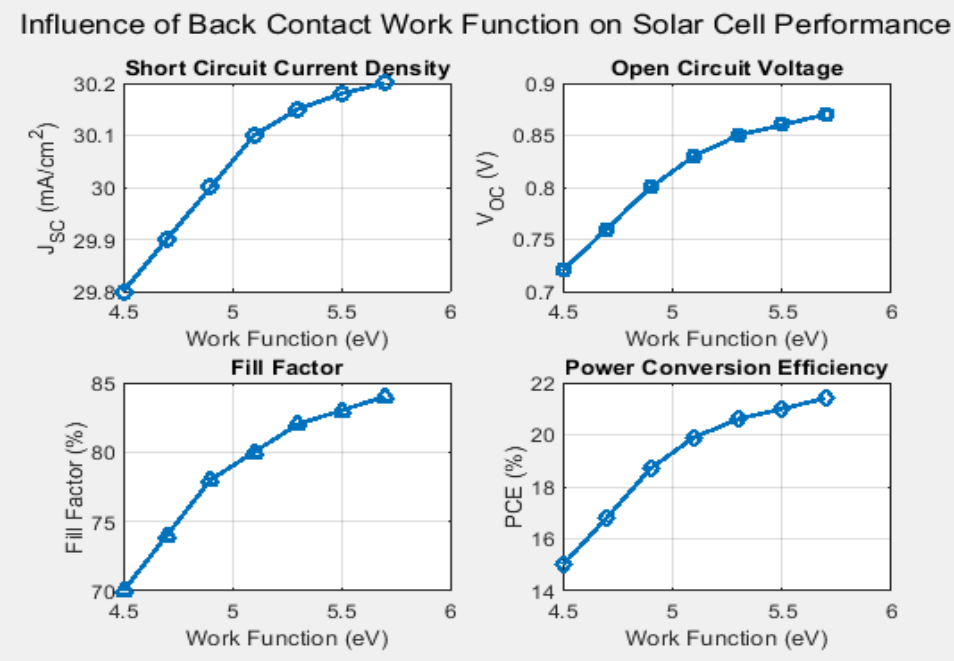

3.7. Effect of Operating Temperature on Device Performance Parameters

The performance of the perovskite solar cell is highly dependent on the operating temperature. This modeling set-up used a base temperature of 300 K, which is the standard operating temperature and provides stable behavior of the devices. To assess thermal performance, the temperature of the device was gradually changed between 300 and 500 K and the performance parameters were tabulated and are presented in the following table. This is caused by the fact that an increase in temperature leads to a severe loss of open-circuit voltage (Voc), fill factor (FF), and power conversion efficiency (PCE). The cause of this degradation is due to carrier concentration, transport dynamics, internal resistive loss, and bandgap modulation of temperature variations [42].

High temperature also causes an extra thermal stress in the structure of perovskite, which facilitates the deformation of the lattice, and the interfaces recombination process is accelerated. These effects enhance the Shockley-Read-Hall (SRH) recombination and decrease the carrier diffusion length, resulting in the higher currents of recombination and internal resistance. That is why, FF and PCE decrease rapidly with temperature. Moreover, an increase in dark saturation current (J0) with temperatures is a contributor to a very significant decrease in Voc because thermally excited carriers destabilize the quasi-Fermi level separation [44].

The simulation output shows that Voc reduces playfully over the temperature interval of 320 K to 500 K to a point of 0.38 V, which indicates the lower capacity of the device to maintain voltages under thermal conditions. Conversely, there is little change in the short-circuit current density (Jsc) values, which is almost steady at approximately 30.03 mA/cm-2, indicating that the amount of photo generated current would hardly depend on changes in temperature at this range. Nevertheless, FF and PCE are very temperature-dependent. At 320 K, the fill factor decreases significantly by 77.17 to 6.69 at 500 K, and it shows that there is higher internal losses at higher temperatures. In line with this, the efficiency of power conversion reduces to 18.67 per cent to 6.69 per cent, which attests to the negative effect of high operating temperatures on the efficiency of the devices.

These results highlight the urgent need of thermal management methods in enhancing the efficiency, stability of the performance and long term stability of perovskite solar cells, especially in a real-life application in the open and high temperature conditions.

Table 10. Influence of Operating Parameters Temperature on Photovoltaic Performance

Temperature 1 (K)	JSC 1 ($mAcm^{-2}$)	FF 1(%)	VOC 1 (V)	PCE 1 1(%)
320	30.05	77.17	0.80	18.67
350	30.04	74.63	0.70	15.82
400	30.03	70.02	0.60	12.67
450	30.03	64.10	0.49	9.56
500	30.03	57.19	0.38	6.69

Figure12. Parameters Temperature on Photovoltaic Performance

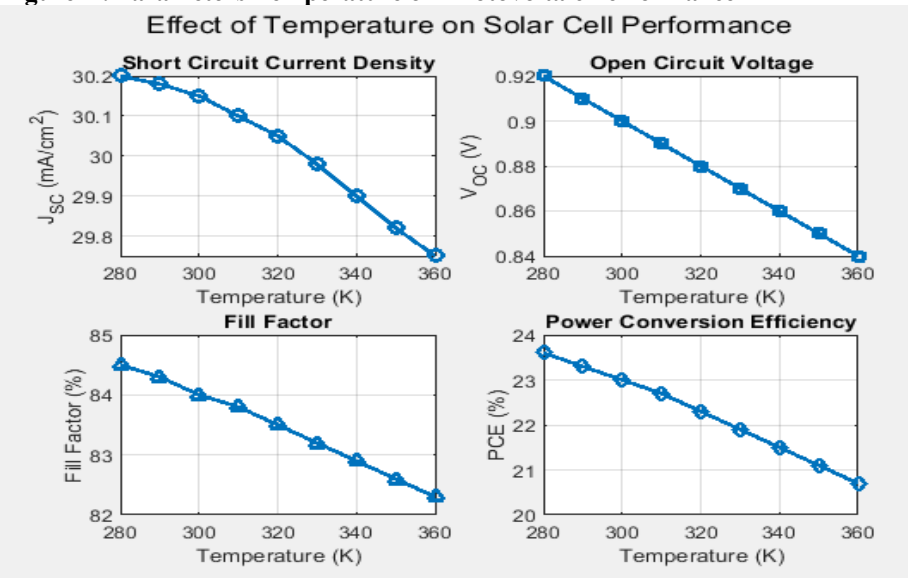

3.8. Influence of Electron Affinity of the HTL and ETL on Device Performance Parameters

The electron affinity of the electron transport layer and the hole transport layer are very vital in the determination of the efficiency of the perovskite solar cell when it is operating. Specifically, a proper adjustment of the electron affinities of the HTL and ETL allows the alignment of the energy-bands of the perovskite absorber, thus allowing the transfer of charges across the transport interfaces effectively. This misalignment caused by the disparity in electron affinity could cause poor performance of device by creating interfacial dislocations that impede the motion of charge carriers. ETL values of 3.9 eV, 4.0 eV, 4.1 e V and 4.2 e V and HTL values of 2.8 e V, 3.0 e V, 3.2 e V and 3.4 e V were simulated and used to determine the impact of the level of electron affinity and the impact of the level of heat of liberation levels on the performance of the device respectively. Each of the combinations was considered systematically to find out what effect each has on key performance measures.

It is shown that the results of the simulation can be optimized to obtain the best performance of the device with high fill factor (FF), open-circuit voltage (Voc) and power conversion efficiency (PCE). This has been improved by the fact that there is a more efficient electron transfer at perovskite/ETL interface that makes the extraction of the charge faster and the interfaces does not incur losses. However, above an ETL electron affinity of 4.2eV, there is poor performance due to undesired band-gap misalignment that leads to structural instability. With respect to this, the HTL electron-efficiency values also take the same trend with the highest performance recorded as the affinity increases in the range of 2.8 to 3.4 eV. This is improved by the fact that an excellent hole transfer between the absorber layer with the HTL is enhanced.

Table 11. Impact of ETL Electron affinity on the performance n parameters

Electron 1Affinity 1(ev)	JSC 1(mAcm-2)	VOC 1(V)	FF (%)	PCE 1(%)
2.90	30.03	0.65	48.7	9.8
3.00	30.40	0.75	58.2	13.65
4.01	30.4	0.81	68.4	17.34
4.2	30.5	0.85	75.1	18.7

Figure 13. Electron affinity on the performance n parameters

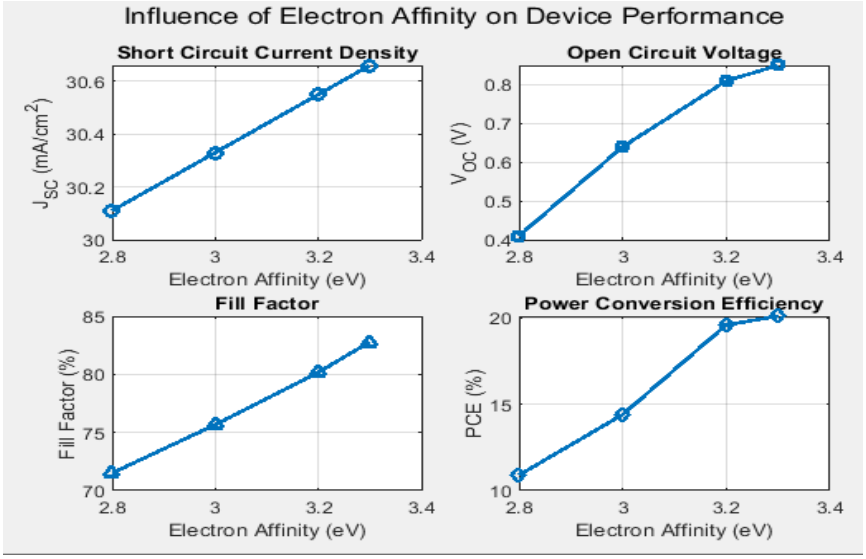

Table 12. Effect of HTL Electron Affinity on Photovoltaic Performance Parameters

The 1Electron 1Affinity 1(ev)	V_{OC} 1(V)	J_{SC} ($mAcm^{-2}$)	FF 1(%)	Power 1conversion 1efficiency 1 1(%)
2.80	0.41	30.11	71.51	10.9
3.00	0.64	30.33	75.67	14.4
3.20	0.81	30.55	80.17	19.6
3.30	0.85	30.66	82.8	20.1

Figure14. Electron Affinity on Photovoltaic Performance Parameters

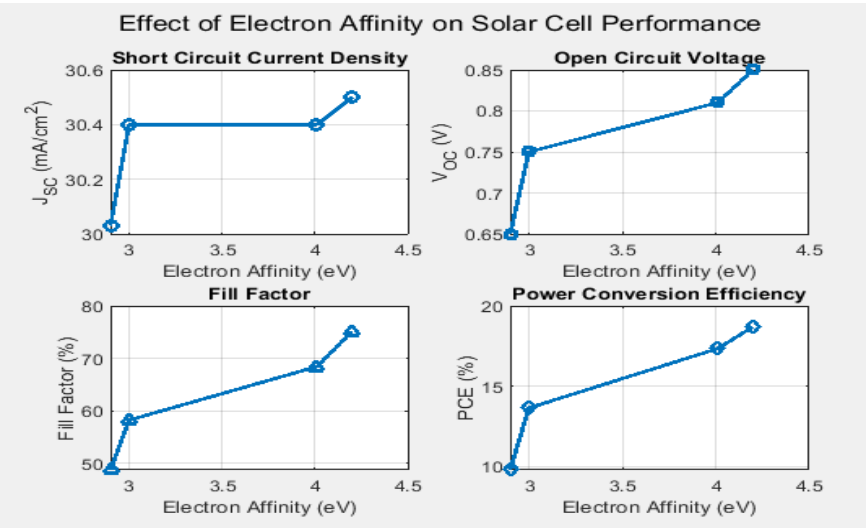

3.9. Influence of Series (R_s) and Shunt Resistance (Rsh) on Device Performance Parameters

The effect of series resistance (Rs) and shunt resistance (Rsh) on the perovskite solar cell performance was thoroughly researched to represent the real operating conditions. These resistive factors are important in determining device efficiency and should hence be factored in a real world performance assessment. In order to measure their effect, parametric simulation was implemented and the performance measures are summarized in the table below. The outcomes show that power conversion efficiency and fill factor strongly decrease with the series resistance, between 1 to 6 Ω cm 2.

Increasing resistance accelerates efficiency degradation, in part due to its negative influence on the fill factor that directly controls the power output that can be attained by the device. Comparatively, changes in open-circuit

voltage (Voc) and short-circuit current density (Jsc) were established to be a relatively small over the same resistance-range. The factors that can cause high series resistance can be low electrode work function alignment and high density of trap states inside the perovskite absorber, which interfere with the efficient charge transport. The shunt resistance, in turn, was negatively related to the performance of the device. Both performance measures also improved with the increase in shunt resistance to 300 Ohm.cm 2 both as compared to 500 Ohm.cm 2, but no further improvement was noted. This is enabled by the fact that this increase in PCE and fill factor is because of minimization of the micro-scale pinholes that normally influence the functionality of the perovskite devices.

Table 13. Effect on of Series Resistance Photovoltaic Performance Metrics

Rs 1(Ohm.cm^2)	Voc 1(V)	Jsc (mAcm^{-2})	FF 1 (%)	PCE 1(%)
1	0.80	30.04	73.92	17.88
2	0.80	30.04	70.73	17.11
3	0.80	30.04	67.57	16.34
4	0.80	30.04	64.45	15.59
5	0.80	30.04	61.37	14.84
6	0.80	30.04	58.33	14.11

Table 14. Impact of Shunt resistance on performance

R_{sh} (Ohm.cm^2)	Voc (V)	Jsc (mAcm^{-2})	FF (%)	PCE (%)
500	0.80	30.05	73.96	17.79
1000	0.80	30.05	75.56	18.23
1500	0.80	30.05	76.10	18.37
2000	0.80	30.05	76.37	18.45
3000	0.80	30.05	76.63	18.52

Figure 15. Impact on of Series Resistance Photovoltaic

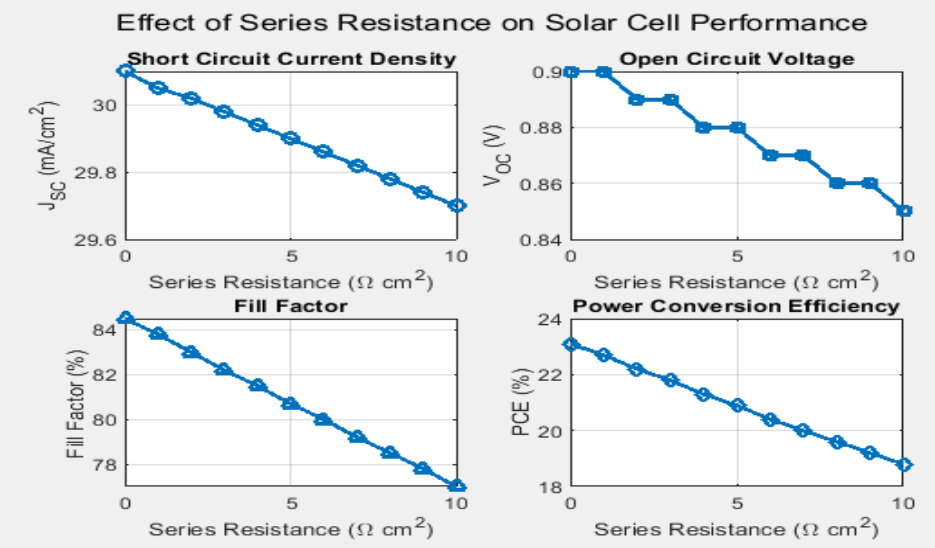

Figure 16. Impact on of Shunt Resistance Photovoltaic

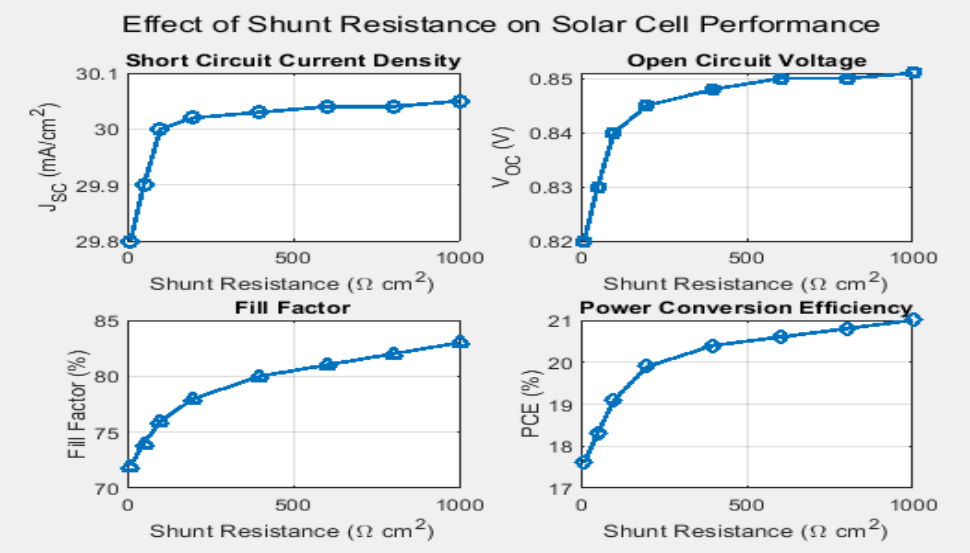

3.10. Analysis of Current–Voltage (J–V) Characteristics

On the basis of the systematic optimization of the main parameters of the device efficiency, the analysis of the current-voltage (J-V) was conducted to assess the electrical characteristics of the perovskite solar cell. The J-V characteristic can be used directly to obtain the basic photovoltaic parameters such as open-circuit voltage (Voc), short-circuit current density (Jsc), and fill factor (FF) that in combination with each other define the power conversion efficiency. A layer of absorber with a thickness of 500 nm is chosen as an optimized configuration to be used in this analysis. Measurements were carried out at an operating temperature of 300 K in standard illumination conditions with an AM 1.5G solar spectrum having an incident intensity that is equal to that of a single sun. In this case, the simulated J-V response produced the most efficient and the total device performance. The final results of the simulation are given below.

- Personal Consumption Expenditure 24.18%
- Voltage of 0.928 V
- Current density of 30.898 mA/cm^2
- Fill factor of 84.39%

The figure presented below illustrates the reduced recombination activity within the perovskite device, with particular emphasis on Shockley–Read–Hall recombination mechanisms and the corresponding recombination current characteristics.

Figure 17. Optimized current–voltage (J–V) characteristics of the perovskite solar cell following performance optimization;

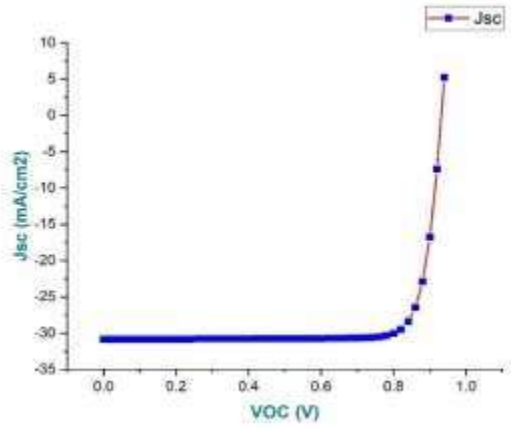

3.9. Assessment of the Quantum Efficiency of the Perovskite

The key parameter that can be used to measure the performance of a particular Perovskite made of tin is its quantum efficiency. The number of electrons that is generated by the light (photon beam) striking a Perovskite material is called quantum efficiency. The quantum efficiency is related to how fast the photo generated charge carriers are caused to generate in the device. This parameter is usually measured as a parameter of the wavelength

of incident photon or alternatively, photon energy. The following graph shows the dependence of wavelength (nm) on QE (percent).
Its quantum efficiency is about 90 percent in the wavelength of 300nm-850nm. This implies that the absorbing layer has a large absorption capacity and the rate of recombination is low. Figures 3 and 4 show the quantum efficiency determined with the photon energy and the quantum efficacy values are higher when the photon energy is 1.8eV and 3.2eV.

Figure 18. Efficacy of Wavelength-Dependent

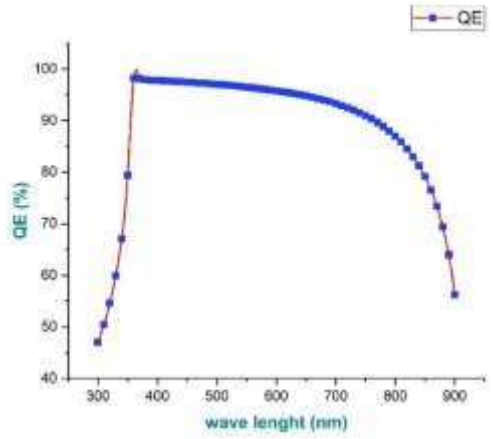

Figure 19. Relationship Between Photon Energy and Quantum Efficiency

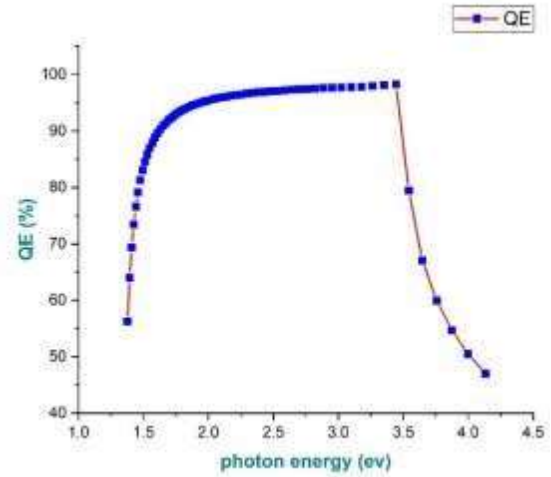

CONCLUSION

This article illustrates a thorough numerical study that has been conducted with the goal of producing an efficient, low-cost and environmentally friendly, lead-free tin-based perovskite solar cell. An architecture of a planar $n-i-p$ device based on the SCAPS-1D simulation platform was developed and optimized which comprised of an FTO/ZnO/CH3NH3SnI3/CuSCN/Au structure. By systematic parametric analysis, the impact of the most important device parameters such as absorber thickness, bandgap energy, electron affinity, acceptor doping concentration, defect density, operating temperature, series resistance and shunt resistance on photovoltaic performance in general were studied.

This optimization approach led to a significant increase in the efficiency of the device with its highest power conversion efficiency of 24.18% and open-circuit voltage of 0.9323 V, short-circuit current density of 30.8360 mA cm -2 and a fill factor of 84.10. Simulated device losses of recombination were significantly low, especially when compared to Shockley-Read-Hall recombination and this means that the charge-carriers were efficiently transported and extracted. Despite the usual architecture constraints of planar device architectures being caused by material compatibility issues, the use of copper(I) thiocyanate (CuSCN) as a hole transport layer improved carrier-extraction efficiency over standard Spiro-Ometad, and minimised interfacial recombination losses associated with tin-based perovskite technological systems.

It is also found that to achieve desirable energy-level alignment and efficient charge collection, close attention and optimization of front and rear metal contacts is necessary. The higher work-function contacts were observed to increases carrier extraction at both interfaces, thus increases device output. All in all, the results have shown that accurate control of the absorber layer thickness, bandgap engineering, and control of bulk and interfacial defect states in addition to the effective use of transport materials and optimization of electrode contacts can contribute greatly to the performance of tin-based perovskite solar cells and its stability. The paper is a very useful contribution to the design principles of the high-efficiency, lead-free perovskite photovoltaic devices that will be utilized in the future and implemented in practice.

Funding: This research received no external funding.
Data Availability Statement: No data set is used in this study.
Declaration Statement: No conflicts of interest declare by the authors.

REFERENCES

[1] A. Kojima, K. Teshima, Y. Shirai, and T. Miyasaka, "Organometal halide perovskites as visible-light sensitizers for photovoltaic cells," Journal of the american chemical society, vol. 131, no. 17, pp. 6050-6051, 2009.
[2] Y. Wu et al., "Highly compact TiO2 layer for efficient hole-blocking in perovskite solar cells," Applied physics express, vol. 7, no. 5, p. 052301, 2014.
[3] P. Vivo et al., "Influence of TiO2 compact layer precursor on the performance of perovskite solar cells," Organic Electronics, vol. 41, pp. 287-293, 2017.
[4] B. Peng, G. Jungmann, C. Jäger, D. Haarer, H.-W. Schmidt, and M. Thelakkat, "Systematic investigation of the role of compact TiO2 layer in solid state dye-sensitized TiO2 solar cells," Coordination Chemistry Reviews, vol. 248, no. 13-14, pp. 1479-1489, 2004.
[5] H. S. Jung and N. G. Park, "Perovskite solar cells: from materials to devices," small, vol. 11, no. 1, pp. 10-25, 2015.
[6] N. J. Jeon et al., "Compositional engineering of perovskite materials for high-performance solar cells," Nature, vol. 517, no. 7535, pp. 476-480, 2015.
[7] J. H. Noh, N. J. Jeon, Y. C. Choi, M. K. Nazeeruddin, M. Grätzel, and S. I. Seok, "Nanostructured TiO 2/CH 3 NH 3 PbI 3 heterojunction solar cells employing spiro-OMeTAD/Co-complex as hole-transporting material," Journal of Materials Chemistry A, vol. 1, no. 38, pp. 11842-11847, 2013.
[8] L. Calió, S. Kazim, M. Grätzel, and S. Ahmad, "Hole-transport materials for perovskite solar cells," Angewandte Chemie International Edition, vol. 55, no. 47, pp. 14522-14545, 2016.
[9] J. Zhang, "Organic Hole Transport Materials for Solid-State Dye-Sensitized and Perovskite Solar Cells," Acta Universitatis Upsaliensis, 2016.
[10] D. Weber, "CH3NH3PbX3, ein Pb (II)-system mit kubischer perowskitstruktur/CH3NH3PbX3, a Pb (II)-system with cubic perovskite structure," Zeitschrift für Naturforschung B, vol. 33, no. 12, pp. 1443-1445, 1978.
[11] D. R. Myers, K. Emery, and C. Gueymard, "Revising and validating spectral irradiance reference standards for photovoltaic performance evaluation," J. Sol. Energy Eng., vol. 126, no. 1, pp. 567-574, 2004.
[12] D. J. MacKay, "Solar energy in the context of energy use, energy transportation and energy storage," Philosophical Transactions of the Royal Society A: Mathematical, Physical and Engineering Sciences, vol. 371, no. 1996, p. 20110431, 2013.
[13] A.-S. Chauvin and M. Grätzel, "Solar energy harvesting," Chimia, vol. 67, no. 3, pp. 113-113, 2013.
[14] H. Müller-Steinhagen and F. Trieb, "Concentrating solar power," A review of the technology. Ingenia Inform QR Acad Eng, vol. 18, pp. 43-50, 2004.
[15] M. Buresch, "Photovoltaic energy systems: Design and installation," New York, 1983.
[16] M. A. Green, "Solar cells: operating principles, technology, and system applications," Englewood Cliffs, 1982.
[17] T. B. Johansson and L. Burnham, Renewable energy: sources for fuels and electricity. Island press, 1993.
[18] D. G. f. Sonnenenergie, Planning and installing photovoltaic systems: a guide for installers, architects and engineers. Earthscan, 2008.
[19] C. Hamaguchi and C. Hamaguchi, Basic semiconductor physics. Springer, 2010.
[20] D. Neamen, Semiconductor physics and devices. McGraw-Hill, Inc., 2002.
[21] S. L. Chuang, N. Peyghambarian, and S. Koch, "Physics of optoelectronic devices," ed: American Institute of Physics, 1996.
[22] M. Burgelman, P. Nollet, and S. Degrave, "Modelling polycrystalline semiconductor solar cells," Thin solid films, vol. 361, pp. 527-532, 2000.

[23] J. Zhao, A. Wang, M. A. Green, and F. Ferrazza, "19.8% efficient “honeycomb” textured multicrystalline and 24.4% monocrystalline silicon solar cells," Applied physics letters, vol. 73, no. 14, pp. 1991-1993, 1998.
[24] M. A. Green et al., "Solar cell efficiency tables (Version 60)," Progress in photovoltaics: research and applications, vol. 30, no. 7, pp. 687-701, 2022.
[25] M. Lazemi, S. Asgharizadeh, and S. Bellucci, "A computational approach to interface engineering of lead-free CH 3 NH 3 SnI 3 highly-efficient perovskite solar cells," Physical Chemistry Chemical Physics, vol. 20, no. 40, pp. 25683-25692, 2018.
[26] L. Lin, L. Jiang, P. Li, B. Fan, and Y. Qiu, "A modeled perovskite solar cell structure with a Cu2O hole-transporting layer enabling over 20% efficiency by low-cost low-temperature processing," Journal of Physics and Chemistry of Solids, vol. 124, pp. 205-211, 2019.
[27] H. Du, W.-C. Wang, and J.-Z. Zhu, "Device simulation of lead-free CH3NH3SnI3 perovskite solar cells with high efficiency*," Chinese Physics B, vol. 25, p. 108802, 2016.
[28] M. Hogan, "Paper Knowledge: Toward a Media History of Documents," Archives and Manuscripts, vol. 42, pp. 307 - 308, 2014.
[29] L. Ma, F. Hao, C. C. Stoumpos, B. T. Phelan, M. R. Wasielewski, and M. G. Kanatzidis, "Carrier Diffusion Lengths of over 500 nm in Lead-Free Perovskite CH3NH3SnI3 Films," Journal of the American Chemical Society, vol. 138 44, pp. 14750-14755, 2016.
[30] Y. Takahashi, H. Hasegawa, Y. Takahashi, and T. Inabe, "Hall Mobility in Tin Iodide Perovskite CH3NH3SnI3: Evidence for a Doped Semiconductor," ChemInform, vol. 44, 2013.
[31] Y. M. Lee et al., "Comprehensive Understanding and Controlling the Defect Structures: An Effective Approach for Organic-Inorganic Hybrid Perovskite-Based Solar-Cell Application," Frontiers in Energy Research, 2018.
[32] C. Devi and R. Mehra, "Device simulation of lead-free MASnI3 solar cell with CuSbS2 (copper antimony sulfide)," Journal of Materials Science, vol. 54, pp. 5615-5624, 2019.
[33] T. Minemoto and M. Murata, "Device modeling of perovskite solar cells based on structural similarity with thin film inorganic semiconductor solar cells," Journal of Applied Physics, vol. 116, p. 054505, 2014.
[34] C. V. Kumar, G. Sfyri, D. Raptis, E. Stathatos, and P. Lianos, "Perovskite solar cell with low cost Cu-phthalocyanine as hole transporting material," RSC Advances, vol. 5, pp. 3786-3791, 2015.
[35] U. Mandadapu, S. V. Vedanayakam, K. Thyagarajan, M. R. Reddy, and B. Jagadeeshbabu, "Design and Simulation of High Efficiency Tin Halide Perovskite Solar Cell," International Journal of Renewable Energy Research, 2017.
[36] A. Iefanova, N. Adhikari, A. Dubey, D. Khatiwada, and Q. Qiao, "Lead free CH3NH3SnI3 perovskite thin-film with p-type semiconducting nature and metal-like conductivity," AIP Advances, vol. 6, p. 085312, 2016.
[37] M. Kevin, W. L. Ong, G. H. Lee, and G. W. Ho, "Formation of hybrid structures: copper oxide nanocrystals templated on ultralong copper nanowires for open network sensing at room temperature," Nanotechnology, vol. 22, p. 235701, 2011.
[38] W. Ming, D. Yang, T. Li, L. Zhang, and M. H. Du, "Formation and Diffusion of Metal Impurities in Perovskite Solar Cell Material CH3NH3PbI3: Implications on Solar Cell Degradation and Choice of Electrode," Advanced Science, vol. 5, 2017.
[39] B. M. Soucase, I. G. Pradas, and K. R. Adhikari, "Numerical Simulations on Perovskite Photovoltaic Devices," 2016.
[40] S. Zandi, P. Saxena, and N. E. Gorji, "Numerical simulation of heat distribution in RGO-contacted perovskite solar cells using COMSOL," Solar Energy, 2020.
[41] C. Yu et al., "Temperature dependence of the band gap of perovskite semiconductor compound CsSnI3," Journal of Applied Physics, vol. 110, p. 063526, 2011.
[42] R. A. J. Janssen, J. C. Hummelen, and N. S. Sariciftci, "Polymer-Fullerene Bulk Heterojunction Solar Cells," MRS Bulletin, vol. 30, pp. 33-36, 2005.
[43] A. Hodsdon et al., "Spectroscopy of neutron-rich P37," Physical Review C, vol. 75, p. 034313, 2007.
[44] Y. Yu and P. Gao, "Development of electron and hole selective contact materials for perovskite solar cells," Chinese Chemical Letters, vol. 28, pp. 1144-1152, 2017.
[45] M. Becker and M. Wark, "Sequentially Deposited Compact and Pinhole-Free Perovskite Layers via Adjusting the Permittivity of the Conversion Solution," Zeitschrift für Naturforschung A, vol. 74, pp. 655 - 663, 2019.
[46] S. A. Moiz, A. N. M. Alahmadi, and M. S. Alshaikh, "Lead-Free FACsSnI3 Based Perovskite Solar Cell: Designing Hole and Electron Transport Layer," Nanomaterials, vol. 13, 2023.

[47] H. Sabbah, "Numerical Simulation of 30% Efficient Lead-Free Perovskite CsSnGeI3-Based Solar Cells," Materials, vol. 15, 2022.
[48] S. Bai et al., "High-performance planar heterojunction perovskite solar cells: Preserving long charge carrier diffusion lengths and interfacial engineering," Nano Research, vol. 7, pp. 1749-1758, 2014.
[49] P. Mahajan, R. Datt, W. C. Tsoi, V. Gupta, A. Tomar, and S. Arya, "Recent progress, fabrication challenges and stability issues of lead-free tin-based perovskite thin films in the field of photovoltaics," Coordination Chemistry Reviews, 2020.